

On the study of momentum correlations in fragmentation in heavy-ion collisions

Sakshi Gautam^{a1} and Rajni Kant^b

^a*Department of Physics, Panjab University, Chandigarh -160 014, India.*

^b*House no. 276, Ward no. 11, Tibbabasti, Patran, Distt. Patiala-147105, Punjab, India.*

The role of momentum correlations in fragmentation is studied within the framework of quantum molecular dynamics model. Our study is carried out by imposing momentum cut in the clusterization algorithm. The study reveals a strong effect of momentum cut in the fragmentation pattern. A comparison with experimental data is also presented. Our theoretical results are in agreement with the experimental data.

¹Email: sakshigautm@gmail.com

1 Introduction

One of the most challenging questions in the present day nuclear physics research is the behavior of nuclear matter in a hot and dense region. This is not only important for nuclear physics, it is also useful for the understanding of the explosion mechanism of supernovae, the formation and structure of neutron stars. The heavy ion collisions at intermediate energies are excellent tool to study the nuclear matter at high density and temperature.

At high excitation energies, the colliding nuclei may break up into several small and intermediate size fragments and a large number of nucleons are also emitted. This phenomenon is known as multifragmentation [1]. A large number of experimental attempts have been carried out ranging from the evaporation of particles to the total disassembly of the dense matter and a situation where excited matter breaks into several fragments. The multifragmentation, is one of the rare phenomena that has attracted major attention in recent years. The physics behind multifragmentation is so complicated that many different theoretical approaches have been developed [1–4]. Since no theoretical model simulates fragments, one needs afterburners to identify clusters. Since correlations and fluctuations are the main features of the molecular dynamics model, the quantum molecular dynamics (QMD) model is very successful in explaining the phenomena of multifragmentation. Since every model simulate single nucleon, one needs to have afterburner to clusterize the phase space. In a very simple picture, we can define a cluster by using space correlations. This method is known as minimum spanning tree (MST) method [5]. In this method, we allow nucleons to form a cluster if their centroids are less than 4 fm. This method works fine when the system is very dilute. At the same time fragments formed in MST method will be highly unstable (especially in central collisions) as there the two nucleons may not be well formed and therefore can be unstable that will decay after a while. In order to filter out such unstable fragments, we impose another cut in terms of relative momentum of nucleons. This method, dubbed as minimum spanning tree with momentum cut (MSTP) method was discussed by Puri *et al.* [6]. Unfortunately this study was restricted to heavier systems like $^{93}\text{Nb}+^{93}\text{Nb}$ and $^{197}\text{Au}+^{197}\text{Au}$ reactions. The role of momentum cut on the fragment structure of lighter systems is still unclear. We aim to address this in present paper. Here we plan to see the role of momentum cut on the fragment structure of lighter colliding systems and also to see the role of colliding geometry on the fragment

structure with momentum cut being imposed.

The present study is carried out within the framework of QMD model [2, 3] which is described in the following section.

2 The Formalism

2.1 Quantum Molecular dynamics (QMD) model

We describe the time evolution of a heavy-ion reaction within the framework of Quantum Molecular Dynamics (QMD) model [2, 3] which is based on a molecular dynamics picture. This model has been successful in explaining collective flow [7], elliptic flow [8], multifragmentation [9] as well as dense and hot matter [10]. Here each nucleon is represented by a coherent state of the form

$$\phi_\alpha(x_1, t) = \left(\frac{2}{L\pi} \right)^{\frac{3}{4}} e^{-(x_1 - x_\alpha(t))^2} e^{ip_\alpha(x_1 - x_\alpha)} e^{-\frac{ip_\alpha^2 t}{2m}}. \quad (1)$$

Thus, the wave function has two time dependent parameters x_α and p_α . The total n-body wave function is assumed to be a direct product of coherent states:

$$\phi = \phi_\alpha(x_1, x_\alpha, p_\alpha, t) \phi_\beta(x_2, x_\beta, p_\beta, t) \dots, \quad (2)$$

where antisymmetrization is neglected. One should, however, keep in the mind that the Pauli principle, which is very important at low incident energies, has been taken into account. The initial values of the parameters are chosen in a way that the ensemble ($A_T + A_P$) nucleons give a proper density distribution as well as a proper momentum distribution of the projectile and target nuclei. The time evolution of the system is calculated using the generalized variational principle. We start out from the action

$$S = \int_{t_1}^{t_2} \mathcal{L}[\phi, \phi^*] d\tau, \quad (3)$$

with the Lagrange functional

$$\mathcal{L} = \left(\phi \left| i\hbar \frac{d}{dt} - H \right| \phi \right), \quad (4)$$

where the total time derivative includes the derivatives with respect to the parameters. The time evolution is obtained by the requirement that the action is stationary under the

allowed variation of the wave function

$$\delta S = \delta \int_{t_1}^{t_2} \mathcal{L}[\phi, \phi^*] dt = 0. \quad (5)$$

If the true solution of the Schrödinger equation is contained in the restricted set of wave function $\phi_\alpha(x_1, x_\alpha, p_\alpha)$, this variation of the action gives the exact solution of the Schrödinger equation. If the parameter space is too restricted, we obtain that wave function in the restricted parameter space which comes close to the solution of the Schrödinger equation. Performing the variation with the test wave function (2), we obtain for each parameter λ an Euler-Lagrange equation;

$$\frac{d}{dt} \frac{\partial \mathcal{L}}{\partial \dot{\lambda}} - \frac{\partial \mathcal{L}}{\partial \lambda} = 0. \quad (6)$$

For each coherent state and a Hamiltonian of the form,

$H = \sum_\alpha \left[T_\alpha + \frac{1}{2} \sum_{\alpha\beta} V_{\alpha\beta} \right]$, the Lagrangian and the Euler-Lagrange function can be easily calculated

$$\mathcal{L} = \sum_\alpha \dot{\mathbf{x}}_\alpha \mathbf{p}_\alpha - \sum_\beta \langle V_{\alpha\beta} \rangle - \frac{3}{2Lm}, \quad (7)$$

$$\dot{\mathbf{x}}_\alpha = \frac{\mathbf{p}_\alpha}{m} + \nabla_{p_\alpha} \sum_\beta \langle V_{\alpha\beta} \rangle, \quad (8)$$

$$\dot{\mathbf{p}}_\alpha = -\nabla_{\mathbf{x}_\alpha} \sum_\beta \langle V_{\alpha\beta} \rangle. \quad (9)$$

Thus, the variational approach has reduced the n-body Schrödinger equation to a set of $6n$ -different equations for the parameters which can be solved numerically. If one inspects the formalism carefully, one finds that the interaction potential which is actually the Brückner G-matrix can be divided into two parts: (i) a real part and (ii) an imaginary part. The real part of the potential acts like a potential whereas imaginary part is proportional to the cross section.

In the present model, interaction potential comprises of the following terms:

$$V_{\alpha\beta} = V_{loc}^2 + V_{loc}^3 + V_{Coul} + V_{Yuk} \quad (10)$$

V_{loc} is the Skyrme force whereas V_{Coul} , V_{Yuk} and V_{MDI} define, respectively, the Coulomb, and Yukawa potentials. The Yukawa term separates the surface which also

plays the role in low energy processes like fusion and cluster radioactivity [12]. The expectation value of these potentials is calculated as

$$V_{loc}^2 = \int f_{\alpha}(\mathbf{p}_{\alpha}, \mathbf{r}_{\alpha}, t) f_{\beta}(\mathbf{p}_{\beta}, \mathbf{r}_{\beta}, t) V_I^{(2)}(\mathbf{r}_{\alpha}, \mathbf{r}_{\beta}) \times d^3 \mathbf{r}_{\alpha} d^3 \mathbf{r}_{\beta} d^3 \mathbf{p}_{\alpha} d^3 \mathbf{p}_{\beta}, \quad (11)$$

$$V_{loc}^3 = \int f_{\alpha}(\mathbf{p}_{\alpha}, \mathbf{r}_{\alpha}, t) f_{\beta}(\mathbf{p}_{\beta}, \mathbf{r}_{\beta}, t) f_{\gamma}(\mathbf{p}_{\gamma}, \mathbf{r}_{\gamma}, t) \times V_I^{(3)}(\mathbf{r}_{\alpha}, \mathbf{r}_{\beta}, \mathbf{r}_{\gamma}) d^3 \mathbf{r}_{\alpha} d^3 \mathbf{r}_{\beta} d^3 \mathbf{r}_{\gamma} \times d^3 \mathbf{p}_{\alpha} d^3 \mathbf{p}_{\beta} d^3 \mathbf{p}_{\gamma}. \quad (12)$$

where $f_{\alpha}(\mathbf{p}_{\alpha}, \mathbf{r}_{\alpha}, t)$ is the Wigner density which corresponds to the wave functions (eq. 2). If we deal with the local Skyrme force only, we get

$$V^{Skyrme} = \sum_{\alpha=1}^{A_T+A_P} \left[\frac{A}{2} \sum_{\beta=1} \left(\frac{\tilde{\rho}_{\alpha\beta}}{\rho_0} \right) + \frac{B}{C+1} \sum_{\beta \neq \alpha} \left(\frac{\tilde{\rho}_{\alpha\beta}}{\rho_0} \right)^C \right]. \quad (13)$$

Here A, B and C are the Skyrme parameters which are defined according to the ground state properties of a nucleus. Different values of C lead to different equations of state. A larger value of C (= 380 MeV) is often dubbed as stiff equation of state. The finite range Yukawa (V_{Yuk}) and effective Coulomb potential (V_{Coul}) read as:

$$V_{Yuk} = \sum_{j, i \neq j} t_3 \frac{\exp\{-|\mathbf{r}_i - \mathbf{r}_j|\}/\mu}{|\mathbf{r}_i - \mathbf{r}_j|/\mu}, \quad (14)$$

$$V_{Coul} = \sum_{j, i \neq j} \frac{Z_{eff}^2 e^2}{|\mathbf{r}_i - \mathbf{r}_j|}. \quad (15)$$

The Yukawa interaction (with $t_3 = -6.66$ MeV and $\mu = 1.5$ fm) is essential for the surface effects. The relativistic effect does not play role in low incident energy of present interest [11].

2.2 Minimum spanning tree (MST) method

The phase space of nucleons is stored at several time steps. The QMD model does not give any information about the fragments observed at the final stage of the reaction. In order to construct the fragments, one needs clusterization algorithms. We shall concentrate here on the MST and MSTP methods.

According to MST method [5], two nucleons are allowed to share the same fragment if their centroids are closer than a distance r_{min} ,

$$|\mathbf{r}_i - \mathbf{r}_j| \leq r_{min}. \quad (16)$$

where \mathbf{r}_i and \mathbf{r}_j are the spatial positions of both nucleons and r_{min} taken to be 4fm.

2.3 Minimum spanning tree with momentum cut (MSTP) method

For MSTP method, we impose an additional cut in the momentum space, i.e., we allow only those nucleons to form a fragment which in addition to equation(16) also satisfy

$$|\mathbf{p}_i - \mathbf{p}_j| \leq p_{min}, \quad (17)$$

where $p_{min} = 150 \text{ MeV}/c$.

3 Results and Discussion

We simulated the reactions of $^{12}\text{C}+^{12}\text{C}$, $^{40}\text{Ca}+^{40}\text{Ca}$, $^{96}\text{Zr}+^{96}\text{Zr}$ and $^{197}\text{Au}+^{197}\text{Au}$ at 100 and 400 MeV/nucleon at $\hat{b} = 0.0, 0.2, 0.4, 0.6$ and 0.8 . We use a soft equation of state with standard energy-dependent Cugon cross section.

In Figure 1, we display the time evolution of $A^{max}[(a),(b)]$, free nucleons [(c),(d)] and LCPs($2 \leq A \leq 4$) [(e),(f)] for the reactions of $^{12}\text{C}+^{12}\text{C}$ at 100 (left panels) and 400 (right) MeV/nucleon. Solid lines indicate the results of MST method whereas dashed lines represent the results of MSTP method. The heaviest fragment A^{max} follows different time evolution in MSTP as compared to MST method. In MST, we have a single big fragment whereas momentum cut gives two distinct fragments which shows realistic picture.

In Figure 1(c) and 1(d), we display the time evolution of free nucleons. We see that for both the energies, MSTP method yields more free nucleons compared to MST method. There is also a delayed emission of nucleons in MST because of no restrictions being imposed. This delayed emission of free nucleons in MST method takes place because of the fact that till 30 fm/c, we have a single big fragment in MST method (See Figure 1(a),(b)). The fragments saturate earlier in MSTP than MST as predicted in Ref. [6].

In figure 1 [(e),(f)], we display the time evolution of LCPs. We see that MST yields more LCPs. The difference between MST and MSTP method increases at 400 MeV/nucleon signifying significant role of momentum correlations at higher incident energies.

In figure 2, we display the time evolution of E_{rat} of free nucleons and LCP's for the reaction of $^{12}\text{C}+^{12}\text{C}$ at central (left panel) and peripheral (right) colliding geometry. For MST and MSTP methods, we find a significant difference between MST and MSTP methods for both free nucleons and LCP's. The difference is more for the central collisions as compared to the peripheral one.

In figure 3, we display the impact parameter dependence of A^{max} , free nucleons, LCPs, and IMFs for the reaction of $^{40}\text{Ca}+^{40}\text{Ca}$ at 100(left panel) and 400 (right) MeV/nucleon. From both figures we see that A^{max} rises with impact parameter for both methods uniformly. The difference increases with impact parameter. This happens because of the fact that we have a bigger spectator matter (from where A^{max} generates) at peripheral collisions geometry. The number of free nucleons decreases with increase in impact parameter for both methods.

The emission of fragments shows that in contrast to central collisions, peripheral collisions does not show drastic changes with method. This happens due to fact that with increase in colliding geometry, the fragments are the remnants of either projectile or target, therefore breaking mechanisms are almost bound and therefore MSTP methods does not give different results.

In figure 4, we display the impact parameter dependence of A^{max} , free nucleons, and LCPs for the reaction of $^{12}\text{C}+^{12}\text{C}$ at 100 (left panel) and 400 (right) MeV/nucleon. We see that in this particular case, the effect of momentum cut on the fragment production enhances with impact parameter (see figure 4(e) and (f)) which is quite different compared to earlier figures. This is because the spectator matter even at peripheral geometries will be very less in such a lighter system and so the fragments are emitted mostly from the participant region, where they are unstable and hence momentum cut plays a role at such geometries.

As a last step, we also compare our results with the experimental data. In fig. 5, we display the charge distribution for $^{197}\text{Au}+^{197}\text{Au}$ reaction at 150 (left panels) and 250 (right) MeV/nucleon at central ($b = 0-3.5$) and semi-central ($b = 0-8$) colliding geometry. The data are taken from Refs. [13–15]. Solid (open) circles represent the results for MST

(MSTP) method. From figure, we see that both MST and MSTP methods obey the qualitative behaviour of charge distribution, though, quantitatively, MST over predicts the data at both the energies and at both colliding geometry. On the other hand, we find that MSTP method matches the data well at both energies and colliding geometries.

4 Summary

Using the quantum molecular dynamic model, role of momentum correlations in fragmentation was studied. This was achieved by imposing cut in the momentum space during the process of clusterization. We find that this cut yields significant difference in the multifragmentation of colliding nuclei. Our findings are independent of the colliding energy of the reaction.

5 Acknowledgement

This work has been supported by a grant from Centre of Scientific and Industrial Research (CSIR), Govt. of India.

References

- [1] M. Begemann-Blaich, Phys. Rev. C **48**, 610 (1993); M. B. Tsang *et al.*, Phys. Rev. Lett. **71**, 1502 (1993); D. R. Bowmann *et al.*, Phys. Rev. Lett. **67**, 1527 (1991); W. Reisdorf *et al.*, Nucl. Phys. **A612**, 493 (1997); W. Bauer, G. F. Bertsch and H. Schulz, Phys. Rev. Lett. **69**, 1888 (1992).
- [2] J. Aichelin, Phys. Rep. **202**, 233 (1991).
- [3] J. Singh, S. Kumar, and R. K. Puri, Phys. Rev. C **62**, 044617 (2000); R. K. Puri and J. Aichelin, J. Comput. Phys. **162**, 245 (2000); Y. K. Vermani, J. K. Dhawan, S. Goyal, R. K. Puri, and J. Aichelin, J. Phys. G: Nucl. Part. Phys. **37**, 015105 (2010); *ibid.* G **36**, 105103 (2009); Y. K. Vermani and R. K. Puri, Europhys. Lett.

- 85**, 62001 (2009); A. D. Sood and R. K. Puri, Phys. Rev. C **79**, 064618 (2009); *ibid.* C **79**, 064613 (2009).
- [4] C. Dorso and J. Randrup, Phys. Lett. **B301**, 328 (1993).
- [5] P. B. Gossiaux *et al.*, Nucl. Phys. A **619**, 379 (1997); R. K. Puri *et al.*, Phys. Rev. C **54**, R28 (1996).
- [6] S. Kumar and R. K. Puri, Phys. Rev. C **78**, 064602 (2008); *ibid.* C **58**, 320 (1998); *ibid.* C **57**, 2744 (1998).
- [7] A. D. Sood *et al.*, Phys. Lett. B **594**, 260 (2004); *ibid.*, Phys. Rev. C **70**, 034611 (2004); *ibid.* C **69**, 054612 (2004); *ibid.* C **73**, 067602 (2006); *ibid.*, Eur. Phys. J A **30**, 571 (2006); R. Chugh *et al.*, Phys. Rev. C **82**, 014603 (2010); S. Goyal *et al.*, Nucl. Phys. A **853**, 164 (2011); *ibid.* Phys. Rev. C **83**, 047601 (2011); S. Gautam *et al.*, J. Phys. G: Nucl. Part. Phys. **37**, 085102 (2010); *ibid.*, Phys. Rev. C **83**, 014603 (2011).
- [8] S. Kumar *et al.*, Phys. Rev. C **81**, 014601 (2010); *ibid.* C **81**, 014611 (2010); V. Kaur *et al.*, Phys. Lett. B **697**, 512 (2011); S. Gautam *et al.*, Phys. Rev. C **83**, 034606 (2011).
- [9] J. Dhawan *et al.*, Phys. Rev. C **74**, 057901 (2006); *ibid.* C **74**, 057610 (2006).
- [10] C. Fuchs *et al.*, J. Phys. G: Nucl. Part. Phys. **22**, 131 (1996); Y. K. Vermani *et al.*, Nucl. Phys. A **847**, 243 (2010); S. W. Huang *et al.*, Prog. Part. Phys. **30**, 105 (2003).
- [11] E. Lehmann *et al.*, Phys. Rev. C **51**, 2113 (1995); *ibid.*, Prog. Part. Nucl. Phys. **30**, 219 (1993).
- [12] R. K. Puri *et al.*, J. Phys. G: Nucl. Part. Phys. G **18**, 903 (1992); *ibid.*, Eur. Phys. J. A **3**, 277 (1998); *ibid.* **A23**, 429 (2005); *ibid.*, Eur. Phys. J. A **8**, 103 (2008); I. Dutt *et al.*, Phys. Rev. C **81**, 064608 (2010); *ibid.* C **81**, 064609 (2010); *ibid.* C **81**, 047601 (2010); *ibid.* C **81**, 044615 (2010).
- [13] C. Kuhn (FOPI collaboration), Phys. Rev. C **48**, 1232 (1993).

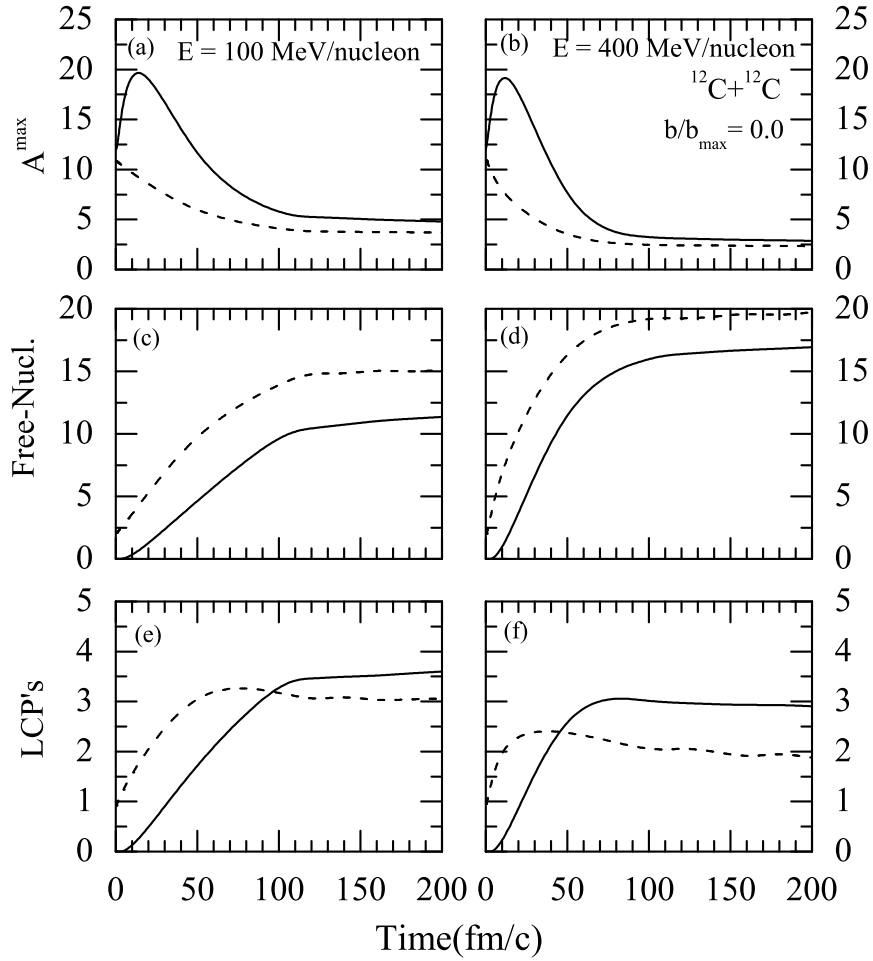


Figure 1: The time evolution of A^{\max} , free nucleons and LCPs for the reaction of $^{12}\text{C}+^{12}\text{C}$ at incident energy of 100 (left panels) and 400 MeV/nucleon (right) with MST and MSTP methods, respectively.

[14] Th. Wienold, Ph.D. thesis, University of Heidelberg (1993), GSI report, GSI-93-28, ISSN 0171-4546.

[15] U. Sodan, Ph.D. thesis, University of Heidelberg, unpublished (1994).

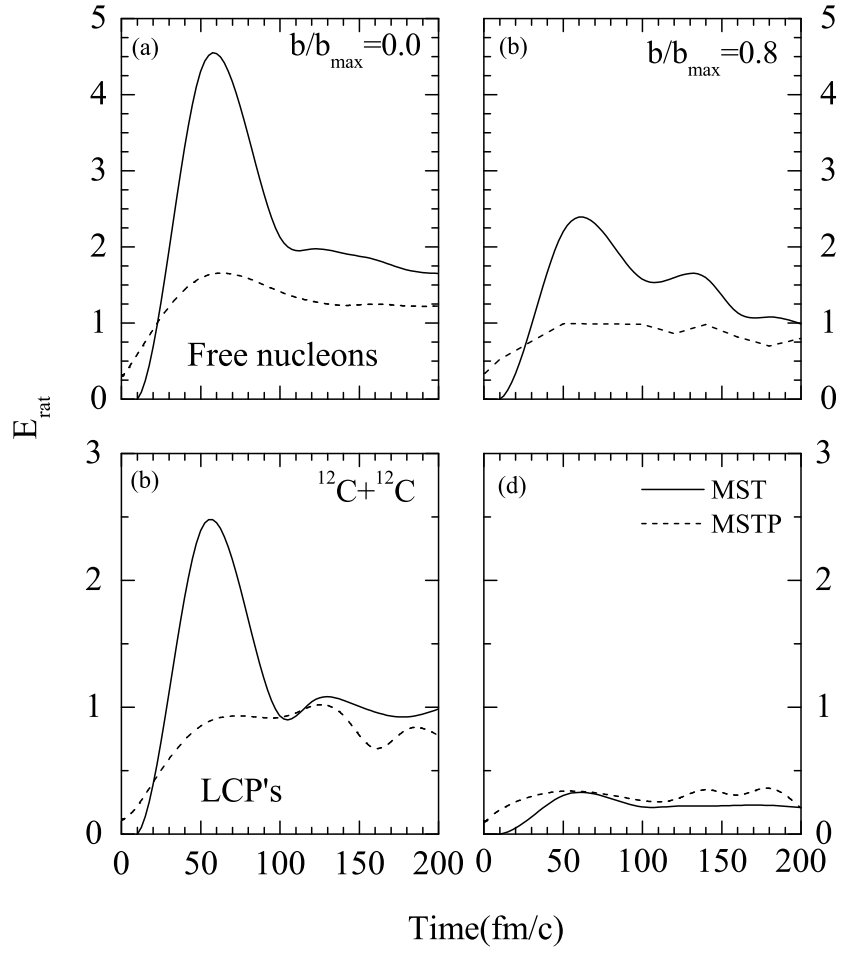


Figure 2: The time evolution of E_{rat} for free nucleons and LCPs for the reaction of $^{12}\text{C}+^{12}\text{C}$ at central (left panels) and peripheral (right) collisions.

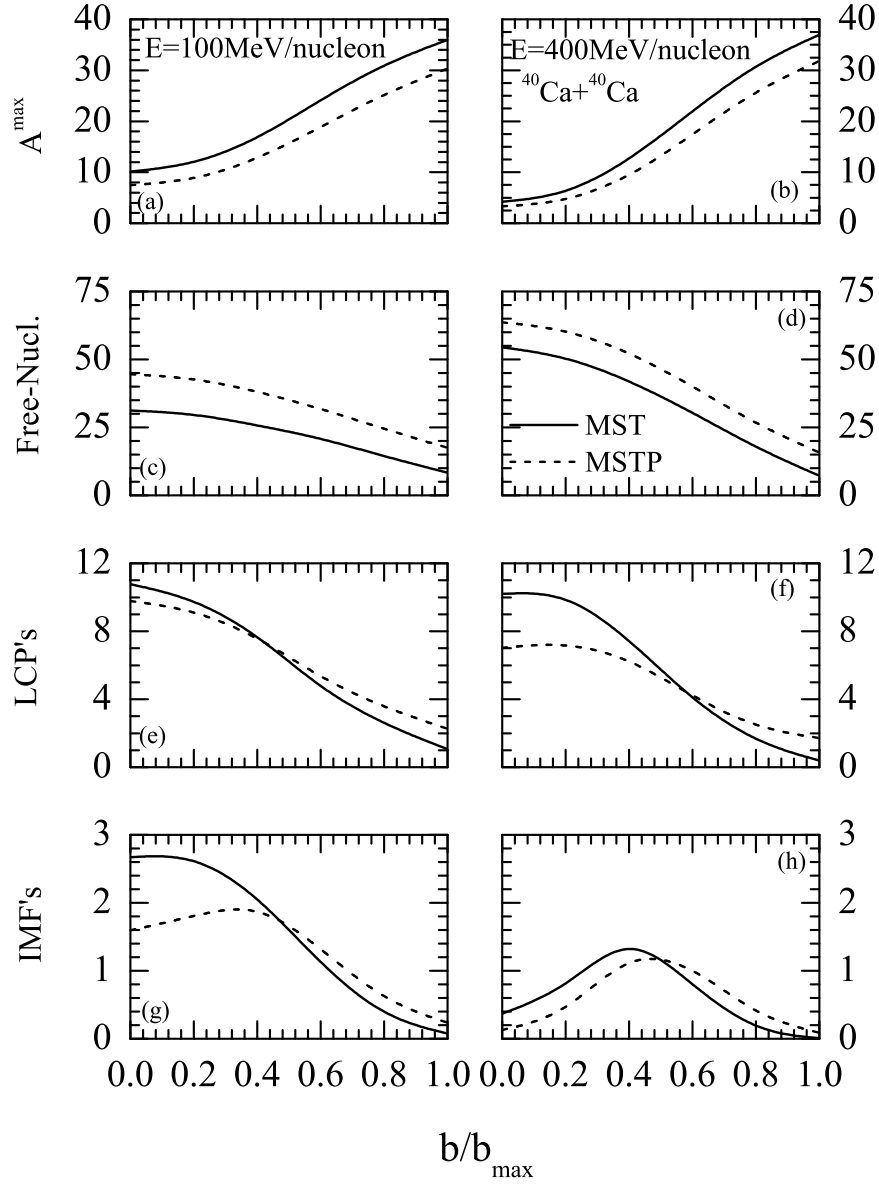


Figure 3: The impact parameter dependence of A^{max} , free nucleons, LCPs and IMFs for the reaction of $^{40}\text{Ca}+^{40}\text{Ca}$ at 100 (left panels) and 400 (right) MeV/nucleon with MST and MSTP methods.

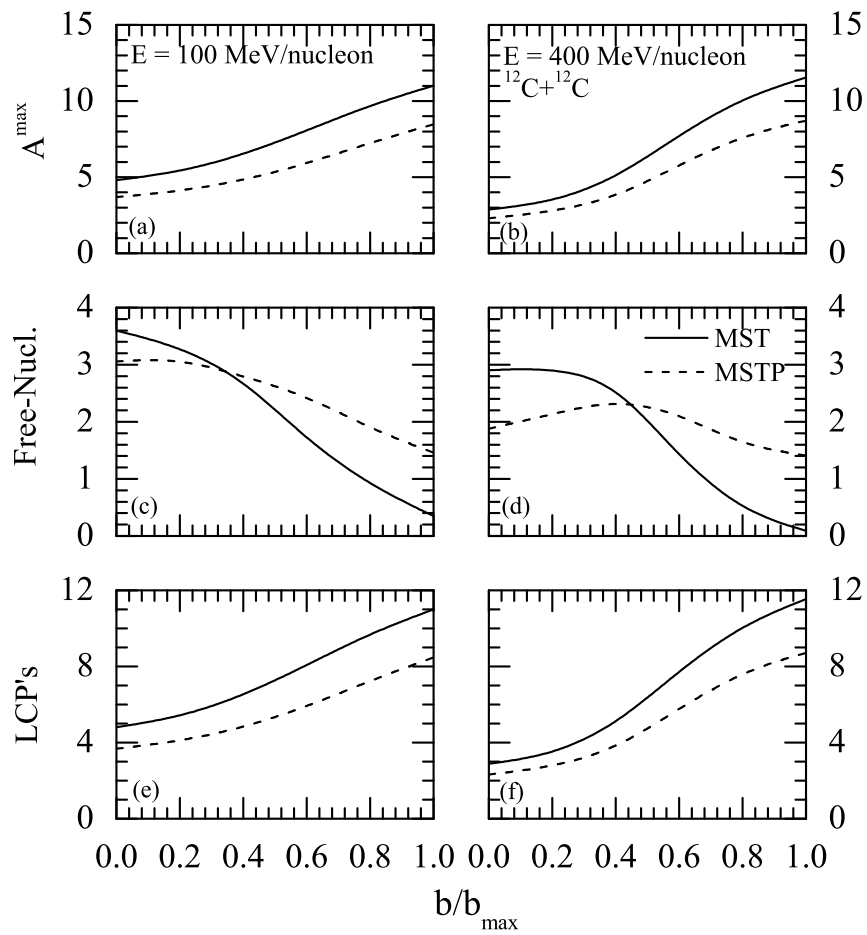


Figure 4: Same as Fig. 3 but for the reaction of $^{12}\text{C} + ^{12}\text{C}$.

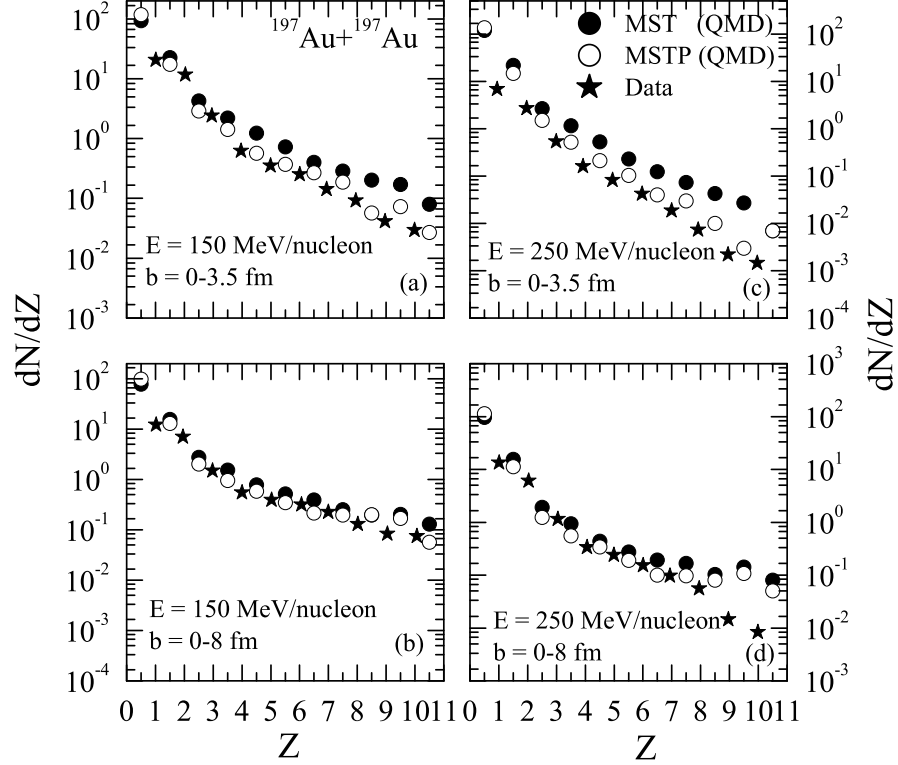


Figure 5: Charge distribution for central and semi-central reactions of $^{197}\text{Au}+^{197}\text{Au}$ reactions. The experimental values for central collisions at 150 MeV/nucleon are taken from Ref. [13] whereas the ones for semi-central collisions at 150 MeV/nucleon are gathered from Ref. [14]. All experimental data for collisions at 250 MeV/nucleon are taken from Ref. [15]. Circles represent our theoretical calculations.